PROTECTED (Up to 5 years)

ALFA-LCP: Advanced Laboratory and Field Arrays – Lab Collaboration Project

Task 11 Nonlinear Ocean Waves and PTO Control Strategy

Task 11.2 Laboratory Experiments for Highly Nonlinear WEC-Wave Conditions

Task 11.3 Improve Nonlinear WEC-Wave Representation in WEC-Sim for High Energy Cases

Data Report for M11.2.3

Bryson Robertson, PhD
Co-Director, Pacific Marine Energy Center
Oregon State University

Ted Brekken, PhD
Professor, Electrical Engineering and Computer Science
Oregon State University

Tuba Ozkan-Haller, PhD
Professor, College of Engineering and College of Earth, Ocean and Atmospheric Sciences
Oregon State University

Solomon Yim, PhD
Professor, Civil and Construction Engineering
Pacific Marine Energy Center
Oregon State University

Pedro Lomonaco, PhD
Director, O.H. Hinsdale Wave Research Laboratory
Pacific Marine Energy Center
Oregon State University

Bret Bosma, PhD
Faculty Research Associate
O.H. Hinsdale Wave Research Laboratory
Oregon State University

Jim Thompson, PhD
Professor, Civil and Environmental Engineering
Applied Physics Laboratory
University of Washington

Nasim Adami
PhD Student, School of Civil and Construction Engineering
Oregon State University

Ali Mohtat
PhD Student, School of Civil and Construction Engineering
Oregon State University

May 2020

Background

The previous DOE deliverable report, due in April 2020, covered some information regarding the experiments performed in December 2019 and February-March 2020 in the Directional Wave Basin at the O.H. Hinsdale Wave Research Laboratory, Oregon State University. This report provides more details on the test setup, instrumentation and sensors, discussion and analysis of the experiment results, and how the conducted experiment could improve the numerical model development.

A brief summary on the experiment is presented here from April 2020 report. The experiments were carried out in the absence and in the presence of a Wave Energy Converter (WEC), including regular and irregular waves using different wave generation and control strategies. The focus was on nonlinear wave conditions and nonlinear PTO control.

Details and analysis of the experiments are presented in the following sections.

Test setup

Experiments presented here were conducted at the Directional Wave Basin (DWB) in O.H. Hinsdale Wave Research Laboratory (HWRL), Oregon State University, during the 2019-2020 academic year. The Directional Wave Basin is 48.8 m long and 26.5 m wide, with 2.1 m high walls and a maximum still water depth of 1.5 m. It is constructed as a reinforced concrete reservoir, with a 15 cm wall and floor thickness. Two vehicle access ramps, 3 m and 2.5 m wide, allow equipment and materials to be transported conveniently into and out of the basin. A bridge crane with a capacity of 7.5 tons spans the length and width of the DWB to position the models and to facilitate instrumentation. Unistrut inserts are placed in rows at 1.22 m spacing to affix specimens and instrumentation throughout the basin. The DWB wave generation system is a multidirectional piston-type wavemaker with 30 independently programmable servomotor-driven points. Each drive point has a maximum stroke of 2 m and a maximum velocity of 2 m/s. The wavemaker is capable of generating repeatable regular, irregular, tsunami, and user-defined waves, and is equipped with an active reflected wave cancellation system. The DWB is also equipped with a removable steel beach with a 1:10 slope as passive wave absorber.

The general objective of the experiments was to generate wave fields with different nonlinearities, using different wavemaker theories. To this end, two sets of tests were conducted, undisturbed (without a WEC) and disturbed (with a WEC) wave tests. The wave conditions were chosen to cover a wide range of intermediate to deep water conditions, as it is mostly the target range of WEC operating settings. The undisturbed experiments were conducted first and then from a chosen set of cases, depending on the safety and operation of the WEC, the disturbed tests. Table 1 and Table 2 are presenting the number of test cases and range of parameters for undisturbed experiments. Table 3 and Table 4 are presenting the number of test cases and range of parameters for disturbed experiments. In each test series, different wavemaker theories were used to examine the accuracy of wave generation. More details of the conducted experiments can be found in April 2020 report.

Table 1: Regular wave tests for undisturbed condition.

Regular waves		
Wavemaker theory	Range of steepness (ak)	Total number of cases
Linear wavemaker theory	0.04-0.4	58
2^{nd}-order wavemaker theory	0.02-0.4	57
NLS wavemaker theory	0.02-0.4	71
Total		186

Table 2: Irregular wave tests for undisturbed condition.

Irregular waves		
Wavemaker theory	Range of steepness (ak)	Total number of cases
2^{nd}-order wavemaker theory	0.02-0.18	7
NLS wavemaker theory	0.02-0.18	7
Total		14

Table 3: Regular wave tests for disturbed condition.

Regular waves		
Wavemaker theory	Range of nonlinearity (ak)	Total number of cases
Linear wavemaker theory	0.02-0.35	7
2nd order wavemaker theory	0.04-0.35	20
NLS wavemaker theory	0.04-0.35	18
Total		45

Table 4: Irregular wave tests for disturbed condition.

Irregular waves		
Wavemaker theory	Range of nonlinearity (ak)	Total number of cases
2nd order wavemaker theory	0.04-0.18	4
NLS wavemaker theory	0.04-0.18	4
Total		8

Tests were conducted in two phases, phase one in Dec 2019 with larger number of wave gauges with main focus on the undisturbed condition, and phase two in Jan 2020 with a combination of disturbed and undisturbed conditions, including PhaseSpace measurements for response measurements of the WEC resulting in a reduction in the number of wave gauges.

The selected WEC for the experiments in this task is the FOSWEC-2. The Floating Oscillating Surge Wave Energy Converter (FOSWEC-2) is a scaled prototype designed for testing at the O.H. Hinsdale Wave Research Laboratory (HWRL), Oregon State University, by Sandia National Laboratories (SNL). The device described in this report is a major redesign of a previous scaled prototype (FOSWEC) last tested in 2016 by SNL (Ruehl et al., 2019). The flaps and parts of the platform were retained while the rest of the device was redesigned and built. Major design changes include the replacement and submersion of the PTO system, with both motor/generator units and power electronics under the water surface, and the change to PVC spars/foam for the buoyancy/ballast of the device. Figure 1 shows a CAD rendering of the new FOSWEC-2 design taken from the test plan document created by SNL for their latest testing. Figure 2 show the FOSWEC-2 in the Directional Wave Basin ready for testing.

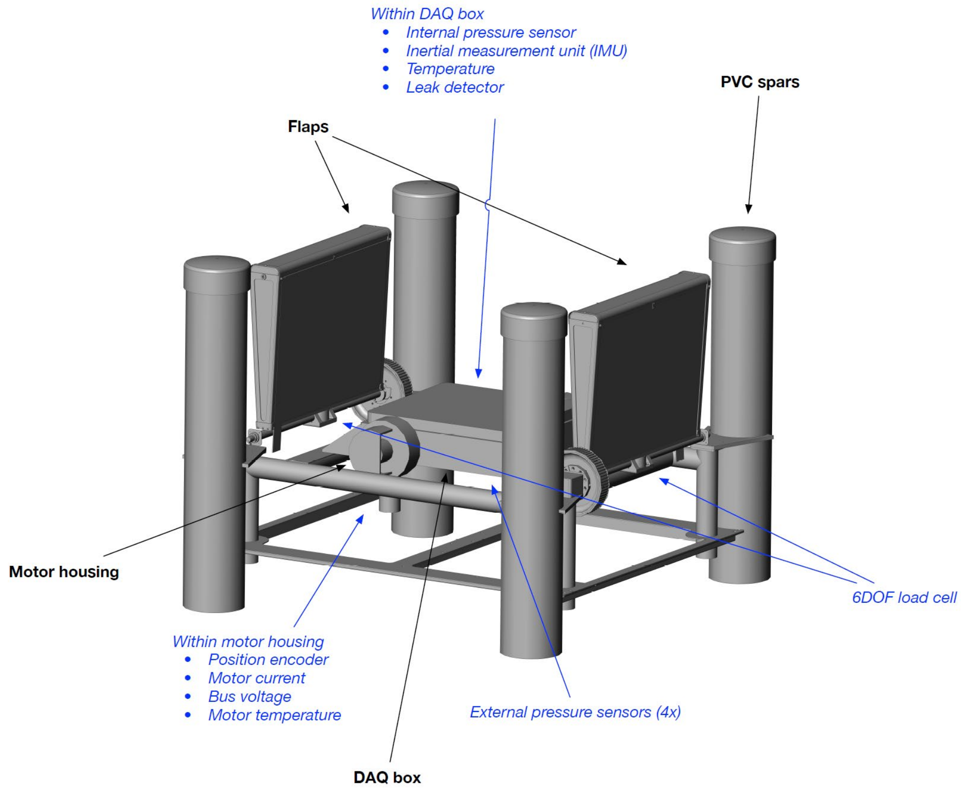

Figure 1: CAD drawing of current FOSWEC-2 model.

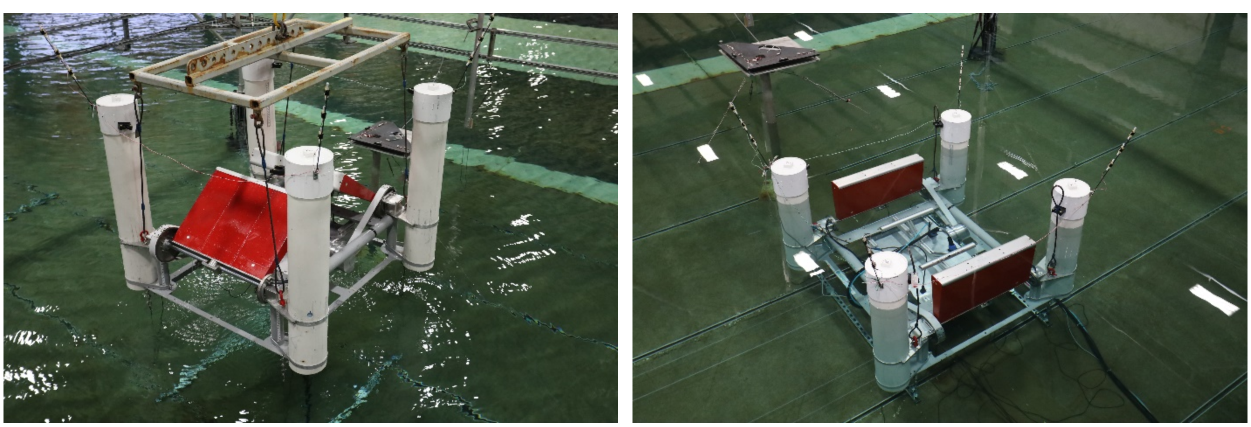

Figure 2: FOSWEC-2 model deployed in the Directional Wave Basin. Left: FOWEC-2 ready to be deployed. Right: FOSWEC-2 ready for testing.

Instrumentation and sensors

As it was mentioned previously, the experiments were conducted in two phases. During phase one, which was mainly concerned with the undisturbed conditions, a total of 16 resistance-based (wgX) and 4 ultra-sonic (uswgX) wave gauges were installed. During this phase, two water depths were considered, i.e. 1.0 m and 1.36 m. The coordinates and names of the deployed wave gauges are presented in Table 5 and the schematic drawing of the instrument layout is shown in Figure 3. As will be shown later, the same 6 m by 6 m frame used in phase 1 was used during the disturbed wave tests to deploy 8 cameras and track the motions of the specimen located at the center of the frame. Moreover, due to the design and operation constraints of the WEC, the space above the model was freed to give access to the overhead crane, which was used to deploy and retrieve the model as needed. The disturbed wave tests (in the presence of the WEC) were executed in February and March, 2020, alternating with the second phase of the undisturbed wave tests.

Table 5: Coordinates of the instruments for the undisturbed wave tests phase 1.

Instruments deployed during the undisturbed wave tests phase 1			
Name	x	y	z
wg1	4.609	-0.039	-
wg2	7.054	-0.023	-
wg3	9.483	-0.031	-
wg4	11.936	-0.023	-
wg5	14.279	-1.404	-
wg6	14.276	-0.006	-
wg7	14.288	1.581	-
wg8	14.663	-2.672	-
wg9	14.714	2.801	-
wg10	15.934	-3.121	-
wg11	15.954	3.126	-
wg12	16.799	-0.006	-
wg13	18.230	-0.027	-
wg14	20.145	-2.822	-
wg15	20.124	2.620	-
wg16	20.517	-0.185	-
uswg1	18.869	-3.313	2.416
uswg2	18.845	3.136	2.406
uswg3	20.621	-1.605	2.398
uswg4	20.628	1.378	2.410

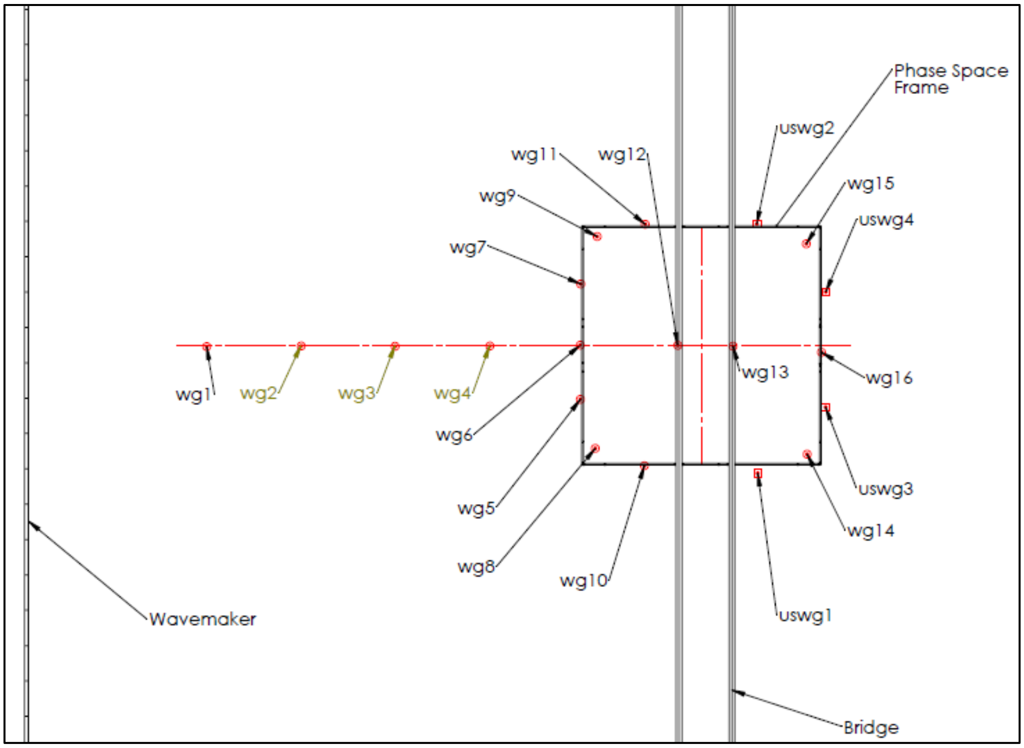

Figure 3: Wave gages layout in the basin during phase 1 of the undisturbed experiments.

During the second phase of the undisturbed tests, 4 columns were required to raise and support the PhaseSpace frame. In this way, motion tracking system was deployed at a higher elevation and remained completely detached from any other structure to ensure a vibration-free structure and eliminate any effect on the measurements. Hence, the number of wave gauges were reduced, and naming were rearranged. During phase two, a total number of 14 resistance-based (scwgX and wgX) and 4 ultra-sonic wave gauges (uswgX) were installed, as shown in Figure 4. Coordinates and names of the deployed wave gauges are also included in Table 6.

Table 6. Coordinates of the instruments for the undisturbed wave tests phase 2.

Instruments deployed during the undisturbed wave tests phase 2			
Name	x	y	z
scwg1	4.601	-0.023	-
scwg2	7.051	-0.022	-
scwg3	9.477	-0.029	-
scwg4	11.914	-0.010	-
wg5	14.368	-1.418	-
wg6	14.380	-0.037	-
wg7	14.391	1.575	-
wg8	14.657	-2.637	-
wg9	14.680	2.684	-
wg10	15.830	-3.012	-
wg11	15.845	2.993	-
wg12	20.032	-2.704	-
wg13	20.049	2.682	-
wg14	20.383	-0.057	-
uswg1	18.898	-3.179	2.359
uswg2	18.797	3.176	2.356
uswg3	20.536	-1.464	2.387
uswg4	20.541	1.510	2.371

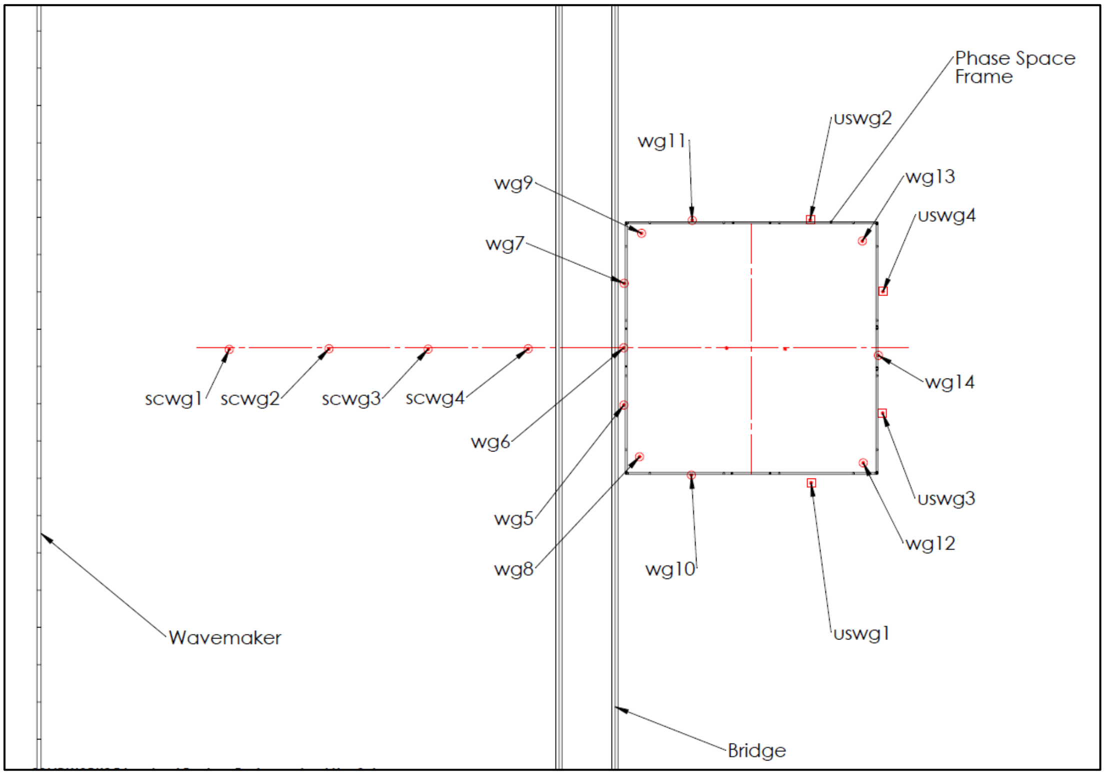

Figure 4: Wave gages layout in the basin during phase 2 of the undisturbed experiments.

In Table 5 and Table 6, the x-axis is the cross-shore coordinate. Its origin (x = 0) is at a vertical plane that best fits the face of the wavemaker piston when it is neutrally positioned. The x-axis is measured in meters and positive onshore (away from the wavemaker). The z-axis is the vertical coordinate. The z-axis origin (z = 0) is at the average elevation of the basin floor. The z-axis is measured in meters and positive upwards. Finally, the y-axis is the alongshore coordinate (parallel to the wavemaker piston). The y-axis origin (y = 0) is at the alongshore centerline of the basin, i.e. halfway between two vertical planes that best fit the basin walls. The y-axis is measured in meters and positive to the left when facing onshore, so that the coordinate system is right-handed.

The Data Acquisition (DAQ) system on the FOSWEC-2 was independent from the HWRL acquisition system, with three synchronization signals logged by both systems. The FOSWEC-2 data was collected on a Speedgoat system using a MATLAB/Simulink environment and EtherCAT communication. Three sampling rates were used for acquisition and control. Figure 5 presents an overview of the data acquisition system of the FOSWEC-2.

PROTECTED (Up to 5 years)

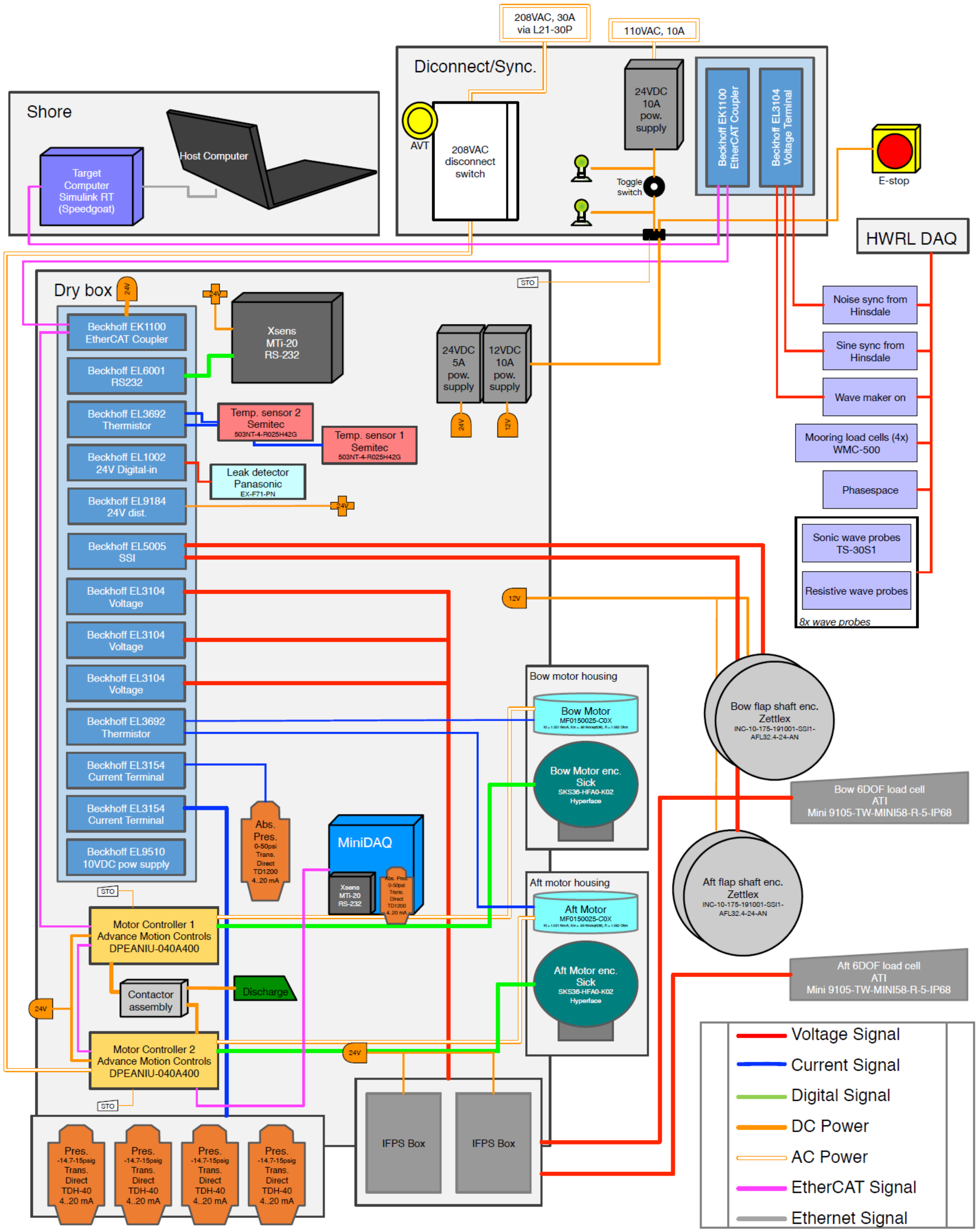

Figure 5: FOSWEC data acquisition system

What follows is a list of relevant measured parameters which describe the operation of the FOSWEC-2. They have been organized based on how they are recorded in the data set. This data set is in the "foswec" directory and arranged by date of test and time of acquisition directories. Data for each trial is in a data.mat file and requires MATLAB to read. Parenthesis are used to help direct to dataset entries.

- HWRL synchronization signals (bridge)
  - HWRL wavemaker start signal (C_waveStart)
    - Goes high when wavemaker starts, goes low when wavemaker stops
  - Sinewave synchronization signal (C_sine)
    - Used for synchronizing FOSWEC and HWRL recorded data
  - Random duration square wave (C_noise)
    - Used for synchronizing FOSWEC and HWRL recorded data
- Platform specific signals (hull)
  - Four pressure sensors (H_P1…H_P4)
  - Absolute pressure (H_Pabs)
  - Temperature (temp)
- Vertical Reference Unit on platform (imu)
  - Rotations (IMU_thx, IMU_thy,IMU_thz)
  - Angular velocity (IMU_wx,IMU_wy, IMU_wz)
  - Accelerations (IMU_accx, IMU_accy, IMU_accz)
- PTO related signals (bow, aft)
  - Motor measured current (I_m)
  - Motor commanded current (I_ref)
  - DC bus voltage (V_DC)
  - Motor measured speed (w_m)
  - Motor measured angle (th_m)
  - Flap measured angle (ssi_f)
  - Flap 6-DOF load cell (ATI_Fx, ATI_Fy, ATI_Fz, ATI_Tx, ATI_Ty, ATI_Tz)

The FOSWEC-2 was designed so the top of the flaps were 2 cm below the SWL, and the selected mooring system considered 4 tension cables to limit heave and restrain surge and sway, while the flaps depicted the largest oscillatory motions relative to the main platform, leading to a TLP-like mooring layout. Tension forces were measured on each of the cables by means of 4 miniature submersible load cells.

6DOF motions (3 linear, i.e. heave, surge, sway, and 3 angular, i.e. yaw, pitch, roll) were captured with the PhaseSpace system by means of 8 stereoscopic cameras mounted on the 6 m by 6 m frame supporting the wave gauges. To measure the motion of the device, PhaseSpace required 4 carbon fiber poles mounted on each corner of the FOSWEC-2, equipped with 3 LEDs blinking with a characteristic signature. The system is able to transform the detected motions non-intrusively with a framerate of 500 samples per second and transform the LED tracking into rigid body 6DOF motions. Measurement of wave gauges and mooring load cells were done with the HWRL DAQ. 6DOF motion tracking was performed in the PhaseSpace server and synchronized with the HWRL DAQ.

The FOSWEC-2 was installed at the center of the 6 m by 6 m frame shown in Figure 4. The coordinates of the 4 load cells and the center of the FOSWEC-2 are listed in Table 7.

Table 7. Coordinates of the load cells and the center of the FOSWEC-2

Load cells			
Name	x	y	z
mooring1	14.330	-2.763	0.079
mooring2	14.351	2.760	0.074
mooring3	20.437	-2.771	0.077
mooring4	20.448	2.713	0.078
Center of the FOSWEC-2			
	17.392	-0.015	-

Analysis of the testing results

The analysis of the experiment results was planned in three main categories: first, the comparison between different wavemaker theories presenting possible improvements from using nonlinear wavemaker theory. Second, the investigation of environmental modeling and wave propagation models applied in WEC simulation programs, using the experimental results. Finally, the analysis of the responses of the WEC under different wave nonlinearity, identifying the response under extreme phenomena, and the PTO performance using nonlinear control strategies. In all the mentioned analysis categories, mainly three approaches are applied, time-domain, frequency-domain, and statistical analysis.

Time-domain analysis covers the time series comparison between the measured generated waves, with different wavemaker theories, and the analytically predicted/propagated waves. The outcome of this comparison is presented by root mean square (rms) error which was computed as the difference between measured and predicted wave time series. Frequency-domain analysis includes the comparison of the spectrum, resulting from different wavemaker theories for waves with different nonlinearities. The spectrum is considered as one of the invariants in the frequency-domain analysis. This approach was mostly emphasized with the irregular wave cases. Statistical analysis of the time series could identify many useful and practical characteristics of the wave field. Using zero-crossing techniques, the time series is discretized into individual wave components which are used to generate wave height probability distributions and detection of the extreme phenomena. The wave height distribution and extreme values are compared between different wave nonlinearities and wave generation theories.

Same approaches are applied for the WEC response data, a simple comparison between the linear and nonlinear wave generation schemes and statistical/frequency analysis. The outcome is to provide evidence, if possible, that the nonlinearity of the wave field plays an important role in the WEC responses and should be included in the numerical model through nonlinear wave propagation models.

Effects of wavemaker theory

Three wavemaker theories were applied during the conducted experiments, linear, second order, and nonlinear Schrödinger (NLS) wavemaker theories (WMT). Among these three theories, the NLS-based wavemaker theory is implemented for the first time generating nonlinear waves in the experimental wave lab facility. The NLS equation is an equation with cubic nonlinearity, describing the water waves behavior in intermediate to deep water condition with $kh \geq 1.36$, where $k=2\pi/L$ is the wavenumber, L is the wavelength and h is the water depth. The maximum range of validity of the NLS equation is found to be about $ak = 0.15$, although larger ak values have been examined during these experiments. The details of the proposed wavemaker theory can be found in previously submitted reports and are not presented here.

Some of the resulting wave field comparisons, using linear, second order, and NLS wavemaker theories are provided in Figure 6 and Figure 7, for the significant wave heights as a function of distance from the wavemaker, for the selected wavemaker theories. The results are from the undisturbed experiment during phase 1 with local water depth of 1.0 m. From these figures, it can be observed that with increasing nonlinearity for each wave period, noticeable differences arise between the linear and 2nd order wavemaker theories, and with the NLS-based wavemaker theory. Also, the region with evanescent modes for NLS-based wavemaker theory is significantly shorter than for the other theories, so the target wave conditions are achieved much faster. Furthermore, all three wavemaker theories provide similar results for the smallest degree of nonlinearity, which is close to the linear condition.

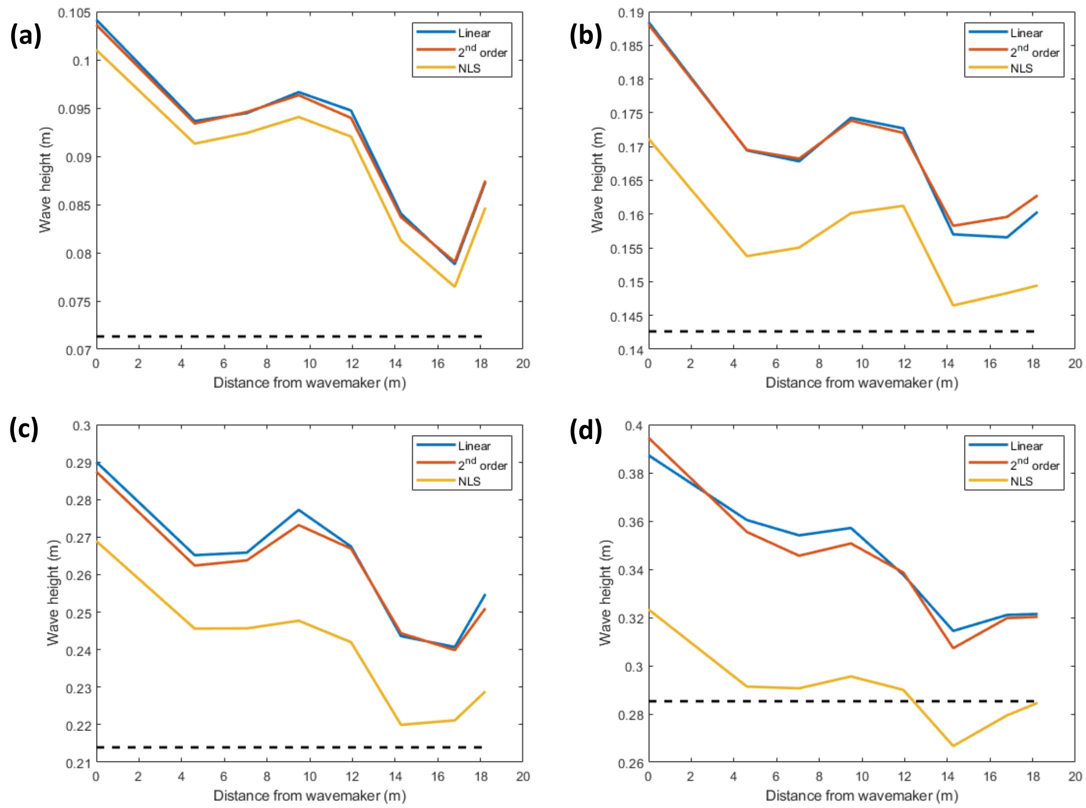

Figure 6: Wave heights of the generated wave field for the case in 1.0 m water depth with $T = 1.8\ s$ and (a) H=0.071, (b) H=0.143, (c) H=0.214, and (d) H=0.285m. The different wavemaker theories, linear, 2nd order, and NLS based generations are compared. On each figure, dashed line presented the target wave height.

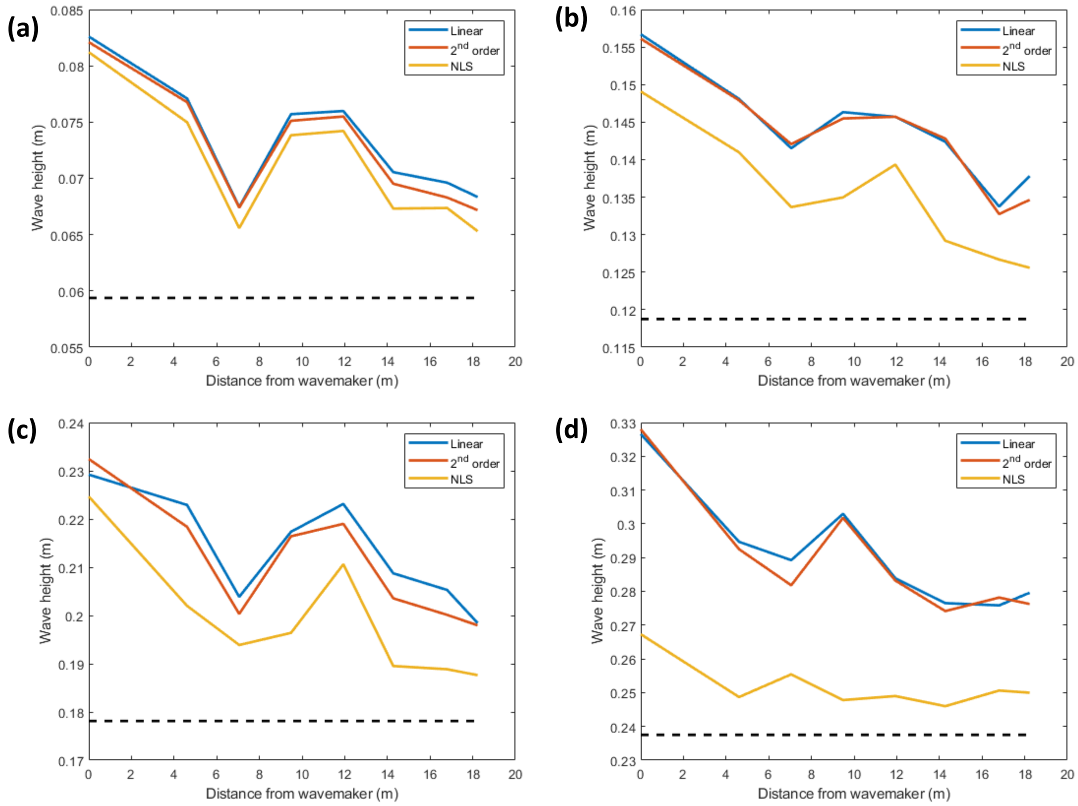

Figure 7: Wave heights of the generated wave field for the case in 1.0 m water depth with $T = 1.6$ s and (a) H=0.059, (b) H=0.119, (c) H=0.178, and (d) H=0.238 m. The different wavemaker theories, linear, 2nd order, and NLS based generations are compared. On each figure, dashed line presented the target wave height.

To compare the resulting generated regular wave fields, the percent difference in wave height is plotted as a function of nonlinearity of the wave field, using different wavemaker theories. The results are presented in Figure 8 for the measurements at WG6 (closest gauge to the WEC location). in the same figure, the average percent differences are shown in dashed lines in same color. On average, the application of NLSWMT reduces the percent difference by more than 5%, which is a major improvement.

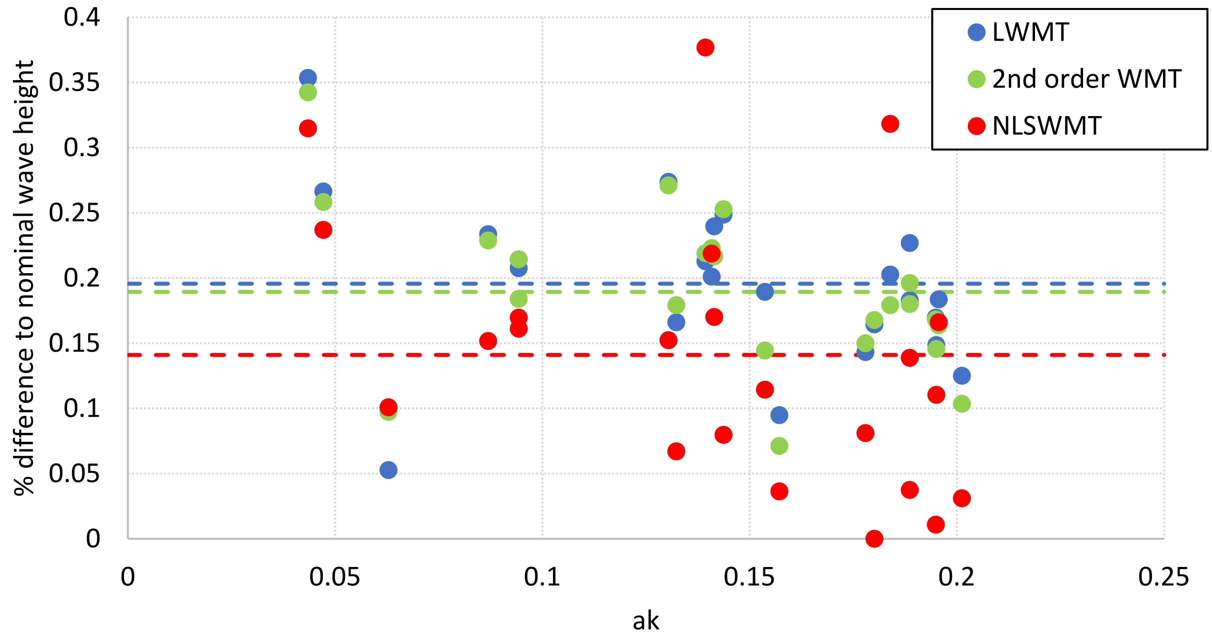

Figure 8: Percent difference in wave height of generated regular wave fields from the nominal values. For each wavemaker theory, the average difference is plotted in the same color dashed line.

The irregular waves were generated following a JONSWAP spectral shape for initial construction of the target time series. The chosen wave conditions were in accordance with the limitations of the WEC and previously done experiments on the FOSWEC-2, therefore, different nonlinearities of 0.18, 0.13, 0.07, and 0.02 were generated. Although the water depth conditions (kh) are not in the domain of validity of the NLS equation, a noticeable improvement was observed in the significant wave height of the generated wave fields. Figure 9 presents the measured significant wave height as a function of distance from the wavemaker, using second order and NLS wavemaker theories. It can be seen from this figure that almost for all nonlinearities, the significant wave heights generated with NLS are closer to the target. The interesting observation is the reduction of the evanescent modes in front of the wavemaker in all cases, which proves the ability of nonlinear wavemaker theory to better capture the true nature of water waves. Further away from the region of validity of NLS equation, the improvements were smaller and the generated wave field characteristics were closer to those generated using 2nd order wavemaker theory.

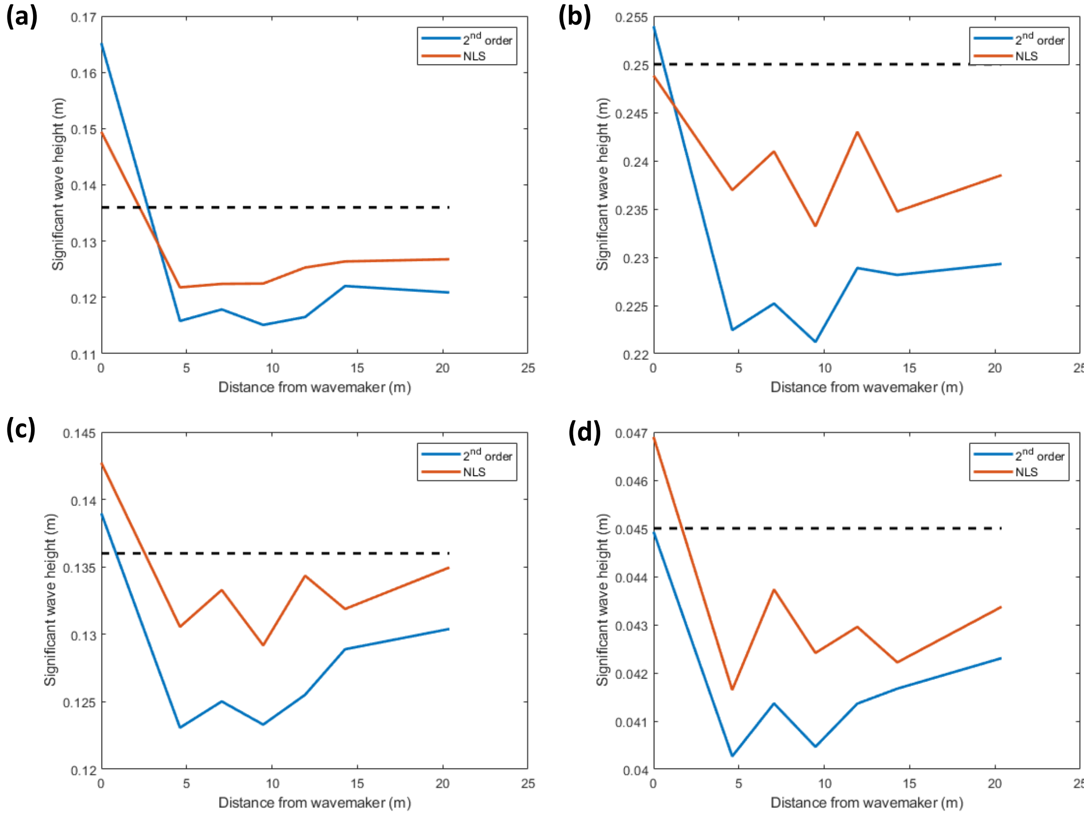

Figure 9: Significant wave heights of the generated irregular waves in 1.36 m water depth with (a) Tp=1.25 s, Hs=0.136, (b) Tp=1.94 s, Hs=0.25, (c) Tp=1.94 s, Hs=0.136, and (d) Tp=1.94 s, Hs=0.045. The different wavemaker theories, 2nd order and NLS based generations are compared. On each figure, dashed line presented the target wave height.

Environmental modeling and prediction models

In the considered WEC numerical simulation model, WEC-Sim, wave elevation time series are assumed to be given at the center of the WEC location. This assumption is not practical in real situations since the measuring devices, e.g. buoys, are located some distance away from the WEC. This may not be of any concern with regular waves, i.e. swells in open ocean, due to the fact that transformation of the time series is a simple phase shift and the distribution of the wave heights and extreme conditions usually doesn't change. But, in case of irregular waves, this transformation is more important since the wave height distribution is changing with location and some extreme phenomena may develop due to simple phase focusing or more complex nonlinear interactions. An example of wave height distribution and its changes with space is presented in Figure 10, for the irregular test case with *Hs=0.136 m , Tp=1.55 s*, using 2nd order and NLS wavemaker theories. The changes in distribution as function of space proves the need for a wave propagation model in the WEC numerical model.

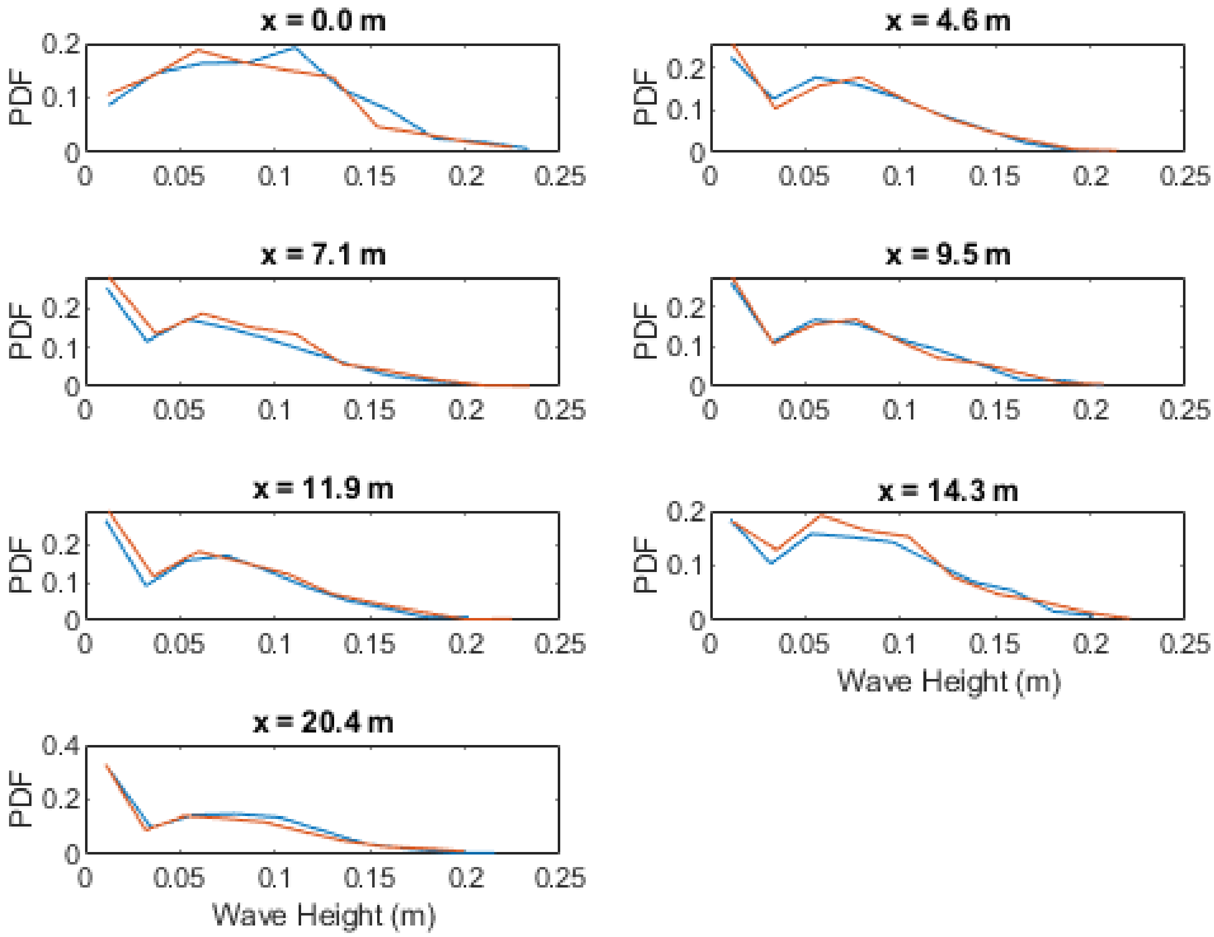

Figure 10: An example of wave height distribution change as a function of distance from the wavemaker. Blue line represents 2nd order and red line NLSWMT.

The wave height distribution at the wave gauge 6 (the closest gauge to the WEC location) was computed for each irregular test case and results are presented in Figure 11. On each figure, the fitted Rayleigh distribution is also shown with the dashed line of the same color. From these figures, the Rayleigh distribution from two different wavemaker theories are closer to one another as the nonlinearity of the generated wave field decreases, as from (a) to (d).

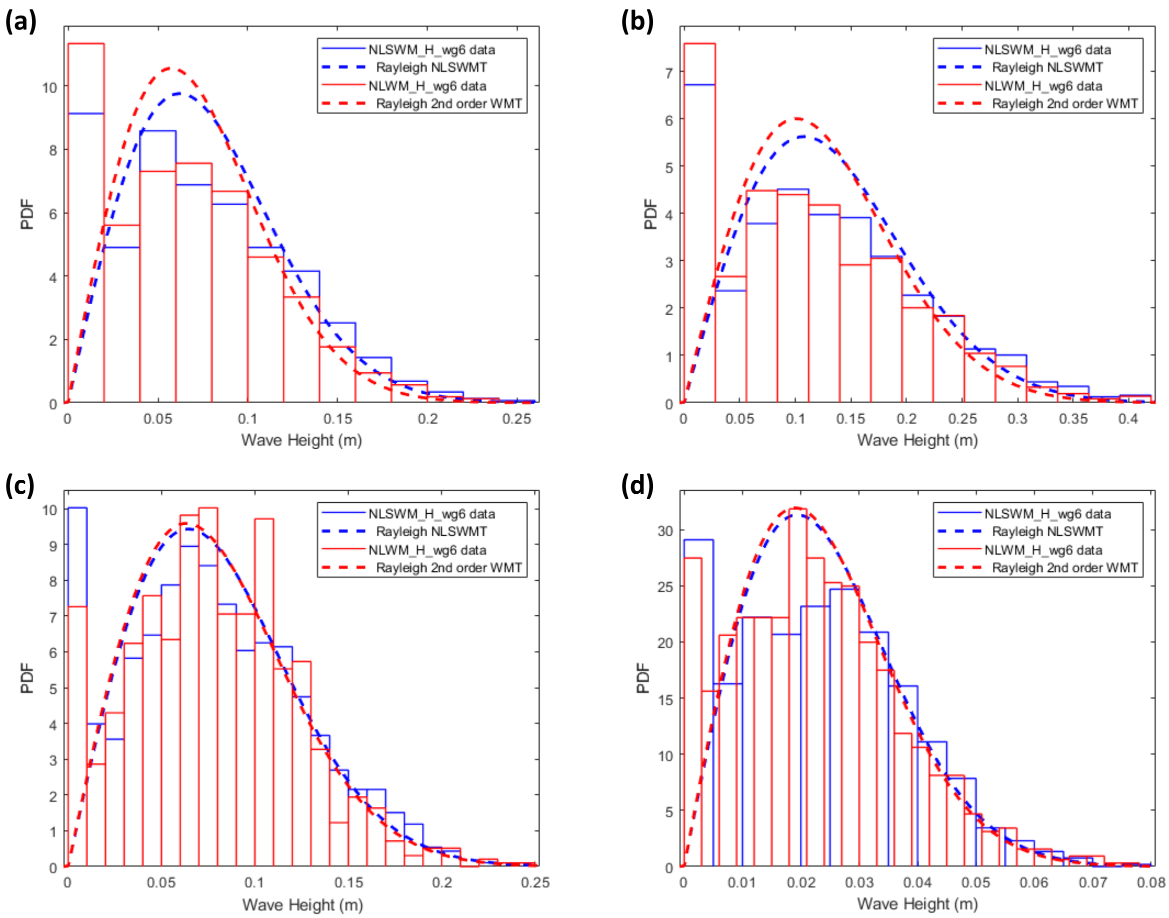

Figure 11: Wave height distribution of the generated irregular waves in 1.36 m water depth with (a) Tp=1.25 s, Hs=0.136, (b) Tp=1.94 s, Hs=0.25, (c) Tp=1.94 s, Hs=0.136, and (d) Tp=1.94 s, Hs=0.045. The different wavemaker theories, 2nd order and NLS based generations are compared. On each figure, dashed line presented the fitted Rayleigh distribution.

As a first approximation for the wave propagation model in numerical WEC simulator, a Fourier based linear wave theory propagation model is implemented on the experimental data. The input time series are the one measured on the wavemaker and the predicted time series at each wave gauge location were compared to the measurements. A point-by-point based root mean square error was developed at each location for each irregular test. The results of rms error are presented in Figure 12. The error of the linear based prediction model show an increasing trend with distance from the wavemaker. It is interesting to observe that the time series generated using NLSWMT proves to be more stable and the errors are smaller for these time series in comparison to those generated using 2nd order wavemaker theory.

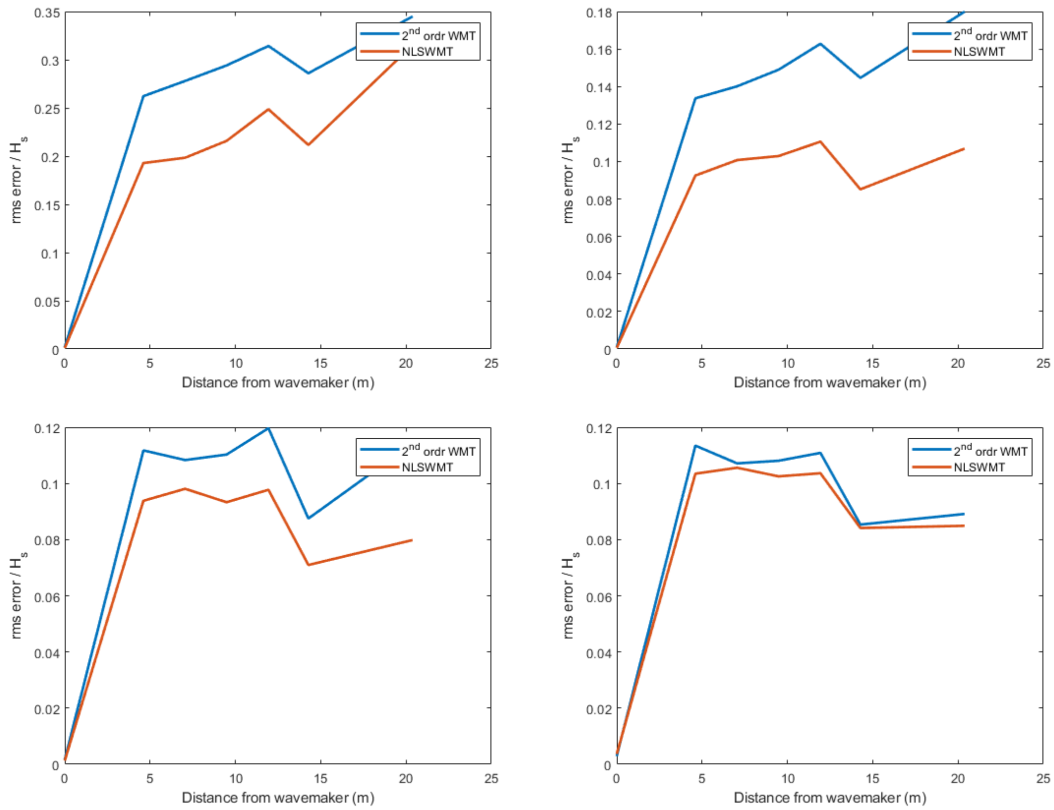

Figure 12: rms error (normalized with significant wave height) of the predicted irregular waves in 1.36 m water depth with (a) Tp=1.25 s, Hs=0.136, (b) Tp=1.94 s, Hs=0.25, (c) Tp=1.94 s, Hs=0.136, and (d) Tp=1.94 s, Hs=0.045.

For highly nonlinear and unstable wave condition, NLS based propagation model can be used to account for deep water instabilities in the time series. Although the linear wave theory-based propagation model provides acceptable results, if the distance between the measuring device and WEC is large, then the errors would become unacceptable and it requires a nonlinear propagation model such as NLS based model. As an example of such unstable wave conditions, a test case was particularly chosen from the phase one of the undisturbed experiments. This type of unstable behavior can be explained by NLS equation. To perform this 2-point prediction, point one (input) is chosen as the measured time series at wg1 (closest WG to the wavemaker) and for point two (target), the furthest wave gauge at a distance of 16 m from wg1 (wg16) is selected. The input time series, along with its envelope, is presented in Figure 13. Two prediction models were executed, linear and NLS, and results were compared as provided in Figure 14. It can be observed that the NLS equation can capture the nonlinear leading instability much better than the linear model predictions.

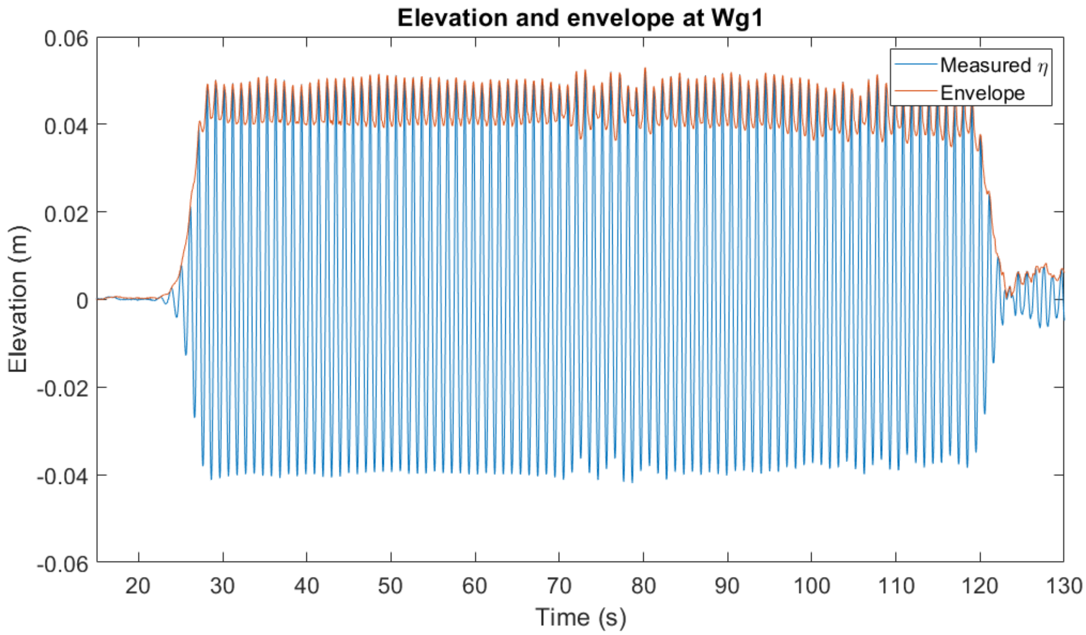

Figure 13: The input time series and envelope function at wg1 (h = 1.0 m, H = 0.1 m, T = 1.0 s).

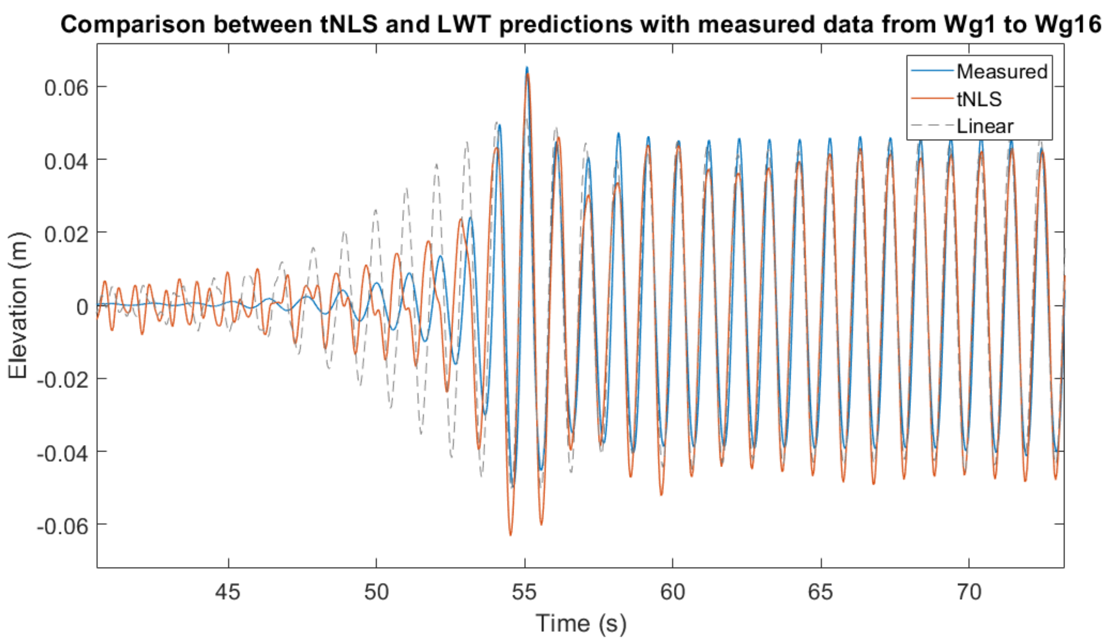

Figure 14: The predicted and measured time series at wg16 (16 m from wg1), using NLS and linear models.

WEC (FOSWEC-2) responses

The excitation source for WEC is the incident waves. Each WEC would respond to the incoming wave field based on its characteristics and mooring mechanism. The WEC included in the presented experiments is FOSWEC-2, details of which was presented previously. FOSWEC-2 has a stand-alone data acquisition system, providing detailed measurements of different responses of the WEC, ranging from 6 DOF forces to flap motions. Such detailed measurements will be used in validations and verifications of the improvements applied on the WEC numerical model, WEC-Sim.

To find the dependency and correlation of the incoming wave field on the response of the WEC, the surge motion of the platform is considered at this section. Two irregular tests with *Hs=0.136 m* and periods of *Tp=1.25, 1.94 s* are examined using frequency domain analysis. The incoming wave time series were adapted from the closest wave gauge readings, WG6. Figure 15 and Figure 16 present the wave and surge time series for different wave conditions and wavemaker theories. Although both test cases have the same significant wave height, Figure 15 for peak period of 1.25 s shows much smaller surge response than Figure 16, with peak period of 1.94 s. It can be reasoned that the natural frequency of the WEC in surge should be close to 0.5 Hz, which resulted in the amplification of the response in the test case with *Tp=1.94 s*.

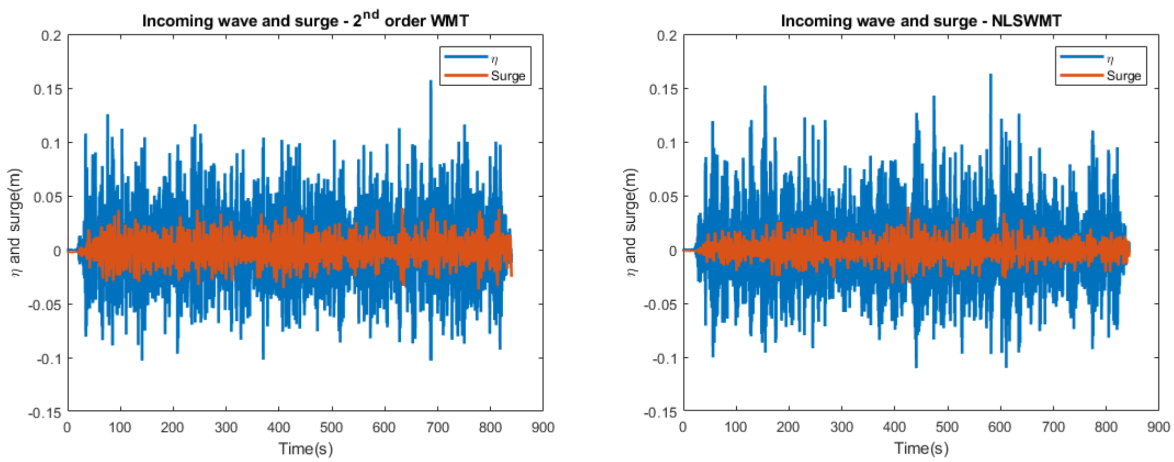

Figure 15: Incoming wave and surge motion for irregular test case with H=0.136 m and T=1.25 s.

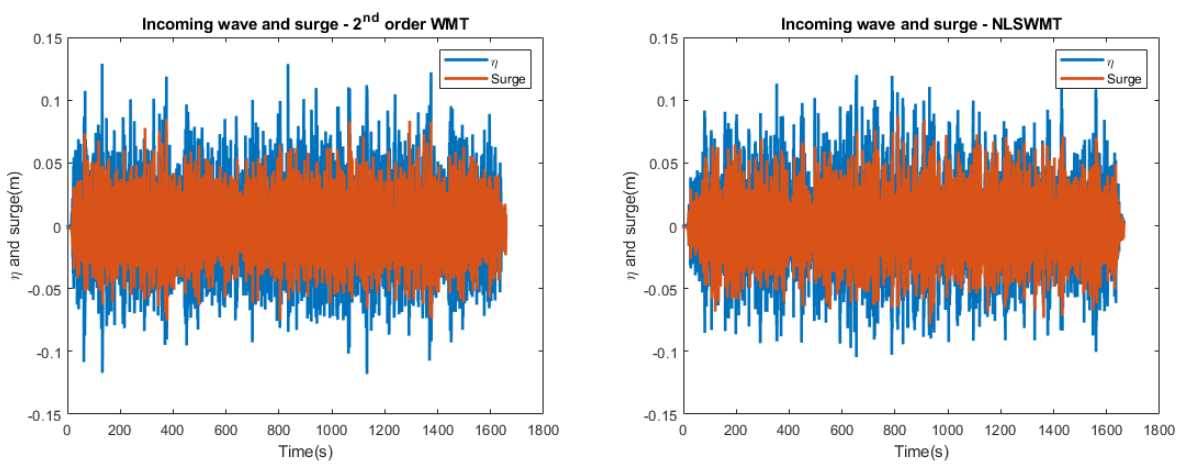

Figure 16: Incoming wave and surge motion for irregular test case with H=0.136 m and T=1.94 s.

To further investigate the response of the WEC in surge, frequency domain analysis (spectral) analysis was performed and results are presented in Figure 17 and Figure 18. From these figures, as the peak frequency of the incoming waves approaches to 0.5 Hz, the responses of WEC in surges amplifies. In general, applying NLSWMT resulted in a more narrow-banded spectrum, which improves the validity of the theories that are based on narrow-band assumption.

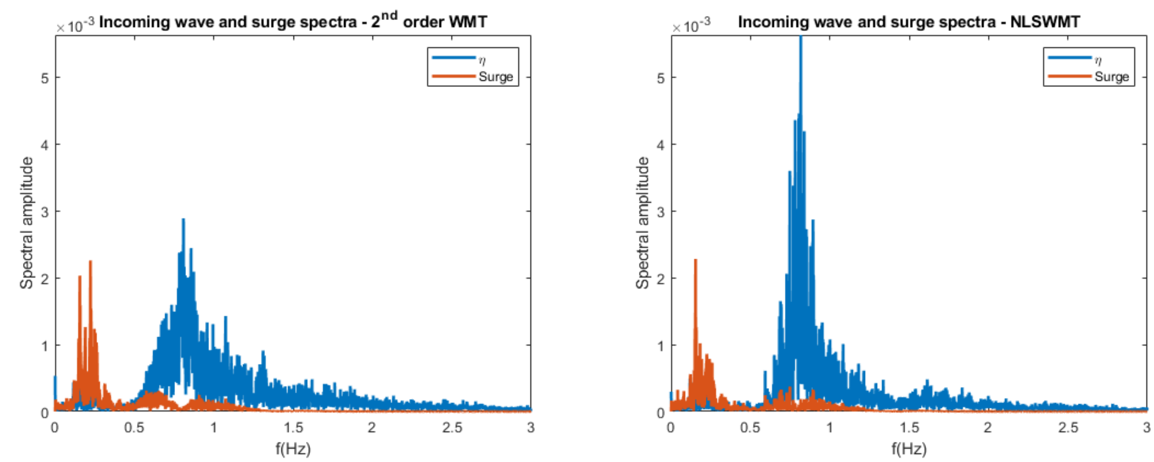

Figure 17: Amplitude spectra of the Incoming wave and surge motion for irregular test case with H=0.136 m and T=1.25 s.

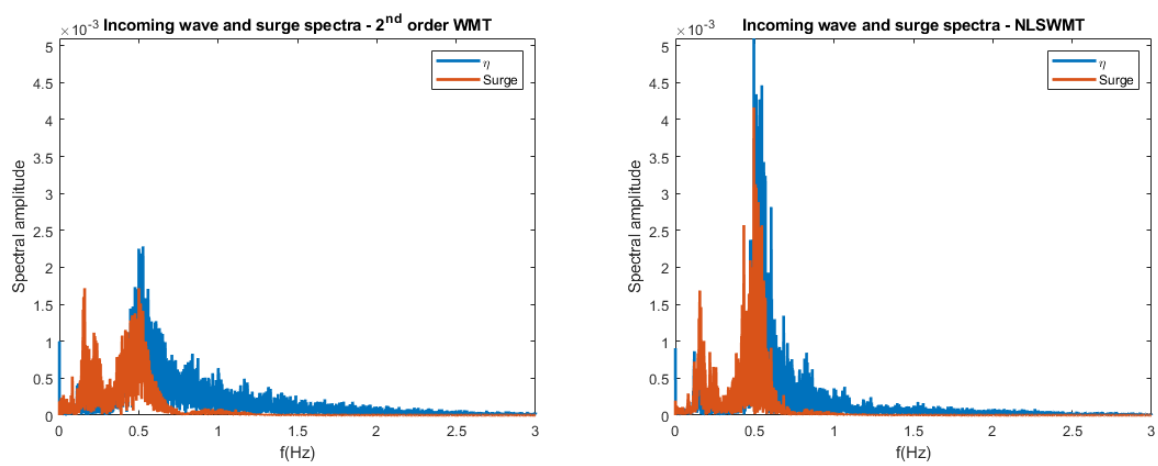

Figure 18: Amplitude spectra of the Incoming wave and surge motion for irregular test case with Hs=0.136 m and Tp=1.94 s.

The maximum surge responses of the WEC, normalized with significant wave height of the incident wave field is presented in Figure 19 and Figure 20 as function of peak period and nonlinearity, respectively. The results are close for 2nd order and NLS wavemaker theories, which shows the validity of system identification results (BEM analysis of the WEC). These results are to be complemented with BEM based analysis results for further examination of WEC behavior.

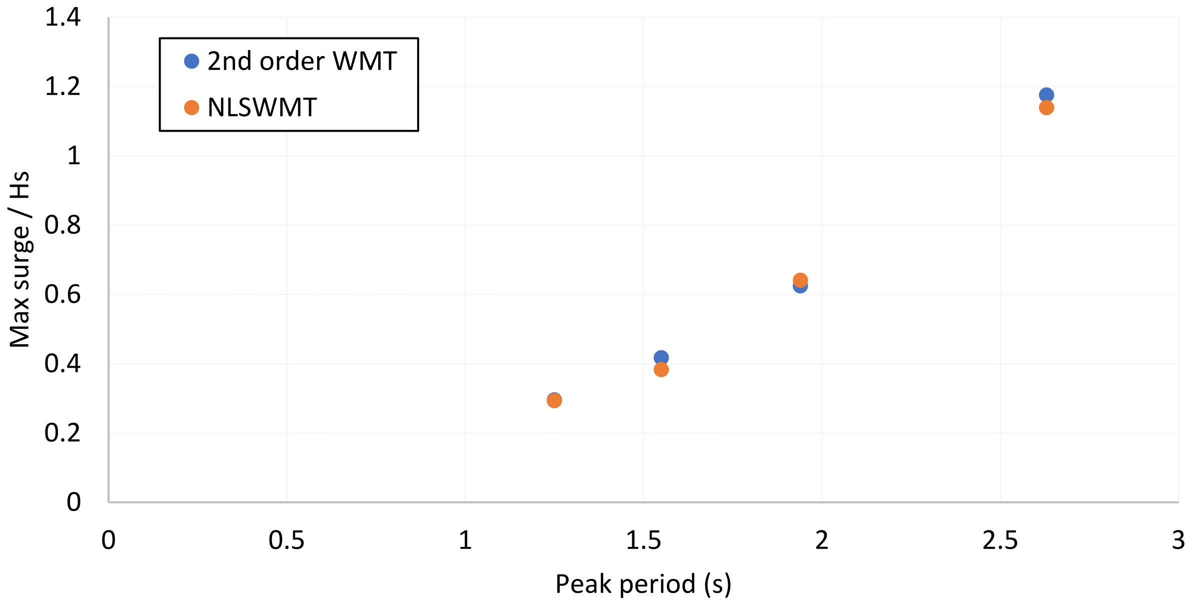

Figure 19: The normalized maximum surge of the WEC with respect to peak period of the wave field.

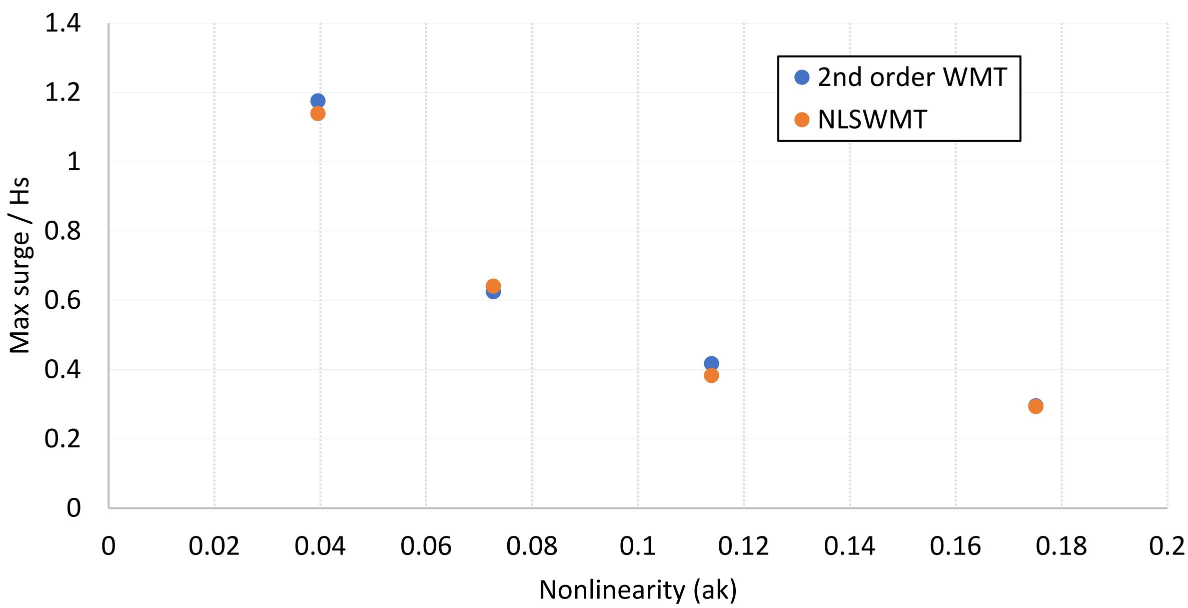

Figure 20: The normalized maximum surge of the WEC with respect to nonlinearity of the wave field.

Discussion and conclusions of the testing results

An overview of the completed and planned analysis of the experimental results were presented in this document. The most important observation was the improvements achieved by implementing NLSWMT in generating nonlinear wave fields, which is consistent for regular and irregular waves. The NLSWMT is a good candidate for any future experiments because of the following observed improvements:

- The generated wave heights were closer to the target wave heights
- The length of the region with evanescent modes was significantly smaller than it is using other wavemaker theories
- The narrow-band characteristics of the target time series was preserved much better
- Generated wave fields were more stable

The linear and nonlinear wave propagation models both provide acceptable results considering the wave field nonlinearity and distance between the measurements and WEC location. These two wave propagation models will be implemented in the WEC-Sim software to improve the wave field approximation and prediction of the model.

Impact of testing results on numerical model development

The conducted experiments provided a detailed database of wave conditions along with the WEC responses. The shortcomings of the current status of WEC-Sim can be evaluated based on the experimental observations and possible improvements will be performed. Results from the current and improved version of WEC-Sim can be verified and validated using the provided experimental data.

Planned analysis steps

The following steps are considered for the final analysis of the measured results:

- Comparison of the generated regular wave field with the associated wave theory and determine the level of agreement.
- Examination of the steady-state duration in the wave basin for regular waves, eliminating the reflection and energy built up effects in the basin.
- Spatial variation of linear and nonlinear spectra for irregular waves and comparing with the target spectral shape.
- Extreme value analysis and wave height distribution examination under different wavemaker theories.
- Sensitivity of the WEC response to the detailed distribution of the wave filed spectrum.